Available online at www.sciencedirect.com
SCIENCE DIRECT®
ELSEVIER
European Journal of Mechanics B/Fluids 22 (2003) 581–601
EUROPEAN JOURNAL OF MECHANICS B/FLUIDS

Free-surface magnetohydrodynamic flow with solidification

Hans O. Åkerstedt, Hans B. Löfgren

Department of Mechanical Engineering, Division of Fluid Mechanics, 97187 Luleå, Sweden

Received 20 February 2001; received in revised form 11 December 2002; accepted 12 June 2003

Abstract

The paper considers an analysis of a liquid metal flow, occurring in the horizontal belt strip casting process. The liquid metal flows over a moving copper belt with a growing solidifying phase beneath the melt. The effect of applying a transverse magnetic field is investigated. A set of three-dimensional shallow water equations is derived. Supercritical flow is assumed and the shallow water equations are solved numerically using a shock-capturing method, which automatically takes care of the possibility of oblique hydraulic jumps.

It is shown that non-uniform conditions introduced in the feeding region give a pattern of steady hydraulic jumps, which propagate downstream and are reflected at the sidewalls. The effect of the magnetic field is to brake the flow and damp the standing hydraulic jump pattern. Different feeding methods are compared and it is shown that the magnetic field erases the initial differences in liquid distribution using different feeding techniques.

1. Introduction

In this paper we consider the liquid metal flow conditions occurring in the casting of thin strips with the horizontal belt strip casting process. The aim of this casting technique is to cast directly thin strips of metal with a thickness ranging from 1 to 15 mm and with typical widths of 0.5–1 m (Nyström et al. [1], Guthrie et al. [2]). In the process the liquid metal is fed onto a horizontally moving conveyor belt. The melt then starts to solidify and the belt withdraws the solidified material with velocity V_{belt}. The velocity of the belt ranges from 0.3 to 1 m/s.

The purpose of the method is to achieve a solidified product with as smooth surface as possible, so that only a minimum of the energy consuming hot rolling process is necessary. The feeding system should therefore be selected with great care in order to minimize the occurrence of waves and instabilities of the liquid metal flow on the belt. In the belt strip casting several feeding techniques have been tested. Tests with feeding through a hole or several holes have given good results (Holmberg [3, 4]). Feeding by a slit (Fig. 1) or down an inclined plane also give quite good results regarding the surface smoothness of the solidified strip, provided the impinging jet has a sufficiently large velocity U_0 of the order of 1 m/s. Using both types of feeding techniques, three-dimensional fluid flow effects are of great importance. In previous theoretical studies of the flow in horizontal belt strip casting two-dimensional models have been considered (Löfgren and Åkerstedt [5–8], Löfgren [9]). A two-dimensional model may be justified if a very wide plane jet is used to feed the liquid metal and especially if the jet is fed obliquely in order to minimize the amount of liquid spread upstream of the jet. In practice however even for a very wide jet, side effects introduce disturbances of the flow, which under certain conditions propagate in the form of oblique steady hydraulic jumps. These jumps are reflected at the sidewalls and the steady waves are only weakly damped by viscous effects.

E-mail address: hans.akerstedt@mt.luth.se (H.O. Åkerstedt).

0997-7546/$ – see front matter
doi:10.1016/j.euromechflu.2003.06.001

Nomenclature

a^*	half the thickness of the impinging jet [m]
$\mathbf{B}^*$	magnetic field [Tesla]
B_0	maximum magnetic field strength [T]
$b_0(X)$	magnetic field in units of maximum magnetic field
$h^*(x^*, y^*)$	free-surface level measured from the upper side of the belt [m]
$\tilde{h}(x, y)$	liquid metal thickness in units of a^*
h_i	heat transfer coefficient [W/m^2·K]
$\bar{h}$	the added thickness of belt, strip and liquid in units of L^*
L^*	belt width [m]
$S^*(x^*)$	thickness of solidified strip [m]
$S(x)$	thickness of solidified strip in units of a^*
T	dimensionless contact resistance $T = \tau\sigma^*/(a^*(\delta + S(X) + \tilde{h}(X, 1/2)))$
T_f	temperature of the liquid metal [K]
T_0	temperature of the cooling medium [K]
U_0	impinging jet velocity [m/s]
u^*	x-component of the velocity [m/s]
v^*	y-component of the velocity [m/s]
U^*	x-component of the free surface velocity [m/s]
V^*	y-component of the free surface velocity [m/s]
V_{belt}	belt velocity [m/s]
x^*	x-coordinate [m]
y^*	y-coordinate [m]
z^*	z-coordinate [m]
x	x-coordinate in units of a^*
y	y-coordinate in units of a^*
z	z-coordinate in units of a^*
X	x-coordinate in units of belt width L^*
Y	y-coordinate in units of belt width L^*
Y^*	boundary layer coordinate $Y^* = (Y - 1/2)/\bar{h}(X, Y)$
α	heat diffusion coefficient [m^2/s]
β	belt velocity in units of U_0
γL^*	characteristic length for the spatial variation of the magnetic field [m]
δ^*	thickness of the cupper belt [m]
δ	thickness of the cupper belt in units of a^*
$\bar{\delta}$	cupper belt thickness in units of $\bar{h}$
Δh_f	latent heat of fusion [J/m^3]
ϕ^*	electrostatic potential [V]
$\bar{\phi}$	electrostatic potential in units of $U_0 B_0 L^*$
ϕ^i	boundary layer potential in units of $U_0 B_0 L^*$
η	boundary layer variable $\eta = (z + \delta)/(\tilde{h}(X, Y) + S(X) + \delta)$
ν	kinematic viscosity [m^2/s]
σ^*	conductivity [Ω^{-1}·m^{-1}]
σ	conductivity in units of conductivity of the copper belt $\sigma = \sigma^*/\sigma_1^*$
τ	contact resistance [Ω·m^2]
ζ	$\zeta = (z - S(x))/\tilde{h}(x, y)$, dimensionless coordinate measured from the bottom of the liquid phase

Dimensionless numbers

$R_m = \mu_0 \cdot \sigma^* U_0 a^*$ magnetic Reynolds number
$R = U_0 a^*/\nu$ Reynolds number
$M^2 = B_0^2 \sigma a^{*2}/(\rho\nu)$ Hartmann number
$F^2 = U_0^2/(g a^*)$ Froude number
$N = B_0^2 \sigma a^*/(\rho U_0)$ interaction number

In a purely two-dimensional free surface flow, it has been shown that plane hydraulic jumps can be avoided if the downstream Froude-number $F^2\beta^3$ is greater than unity (Löfgren and Åkerstedt [5]). (Here the Froude-number is defined as $F^2 = U_0^2/ga^*$ where U_0 is the initial velocity of the jet and a^* is half the initial thickness of the jet. $\beta = V_{\text{belt}}/U_0$ is the dimensionless belt speed.) For this case the flow is everywhere supercritical. In a three-dimensional flow however oblique jumps are possible even if $F^2\beta^3 > 1$. In the direct strip casting process considered here the values of β ranges approximately from 0.3 to about 1 (Guthrie et al. [2]).

We note however that there is another similar casting technique called spin casting (Steen and Karcher [10]), in which the value of β is an order of magnitude larger and the solidified product is thinner, ranging from 0.1–1 mm.

In previous studies (Löfgren and Åkerstedt [5,6]) it has been shown that an application of a transverse magnetic field is favorable for the flow conditions in strip casting. A transverse magnetic field brakes the flow and it also has a large stabilizing effect on waves and instabilities. For the three-dimensional case to be considered in the present paper, the magnetic field also has a dissipating effect on the oblique steady waves. The application of a magnetic field, however, also leads to an induced non-uniform electric field in the entrance region of the magnetic field. This effect also needs a three-dimensional treatment. The inhomogeneous electric field in combination with the transverse magnetic field give a non-uniform braking effect of the liquid, with a stronger braking effect in the more central part of the flow. A side force is also generated which gives a confining effect at the entrance.

The purpose of the present paper is an analysis of the strip casting process including three-dimensional effects. We also include the effects on the flow of a solidifying growing solid phase beneath the melt. The case of no superheat is considered

for which the solidification problem can be treated separately from the fluid flow. The treatment of the free-surface flow is simplified using a shallow water model, in which the boundary layer equations are averaged over the depth of the liquid metal. This results in a system of equations with three dependent variables, the liquid thickness $h^*(x^*, y^*)$, and the surface velocity in the casting x-direction $U^*(x^*, y^*)$ and the surface velocity in the y-direction $V^*(x^*, y^*)$.

The organization of the paper is as follows. In Section 2.1 we consider the flow geometry and the derivation of the shallow water equations. Effects due to solidification are introduced in Section 2.2. The effect of the applied transverse magnetic field is discussed in Section 2.3. The numerical method used to solve this set of equations is briefly discussed in Section 3. For more details of the numerical method the reader may refer to Appendix. Results of the numerical calculations are presented in Section 4. The paper ends with conclusions in Section 5.

2. Basic equations

2.1. Shallow-water theory

We consider the kind of flow that arises after feeding the liquid by a plane jet, impinging vertically or obliquely onto the belt. Generally the flow after the impinging region is characterized by large velocity and shallow depth for that part of the liquid which is spread directly into the casting direction and a liquid moving slower and with larger thickness at the flanks. The latter part originates from the part of the jet, which is initially spread in the direction opposite of the casting direction. (See Fig. 1.) A transverse magnetic field is applied at a position close to the impinging jet.

To simplify the treatment of the free surface flow we consider a shallow water model. This means that we perform an average of the three-dimensional boundary layer equations over the depth of the liquid. Averaging the continuity equation then gives

$$\frac{\partial}{\partial x^*}\int_{S^*(x^*)}^{h^*(x^*,y^*)} u^*\,\mathrm{d}z^* + \frac{\partial}{\partial y^*}\int_{S^*(x^*)}^{h^*(x^*,y^*)} v^*\,\mathrm{d}z^* + u^*\left.\frac{\partial S^*}{\partial x^*}\right|_{z^*=S^*(x^*)} = 0. \tag{2.1}$$

Here $z^* = h^*(x^*, y^*)$ is the position of the free surface and $z^* = S^*(x^*)$ is the position of the solidification front, both with reference to $z^* = 0$ as the upper side of the belt. The relatively small amount of solidification on the sidewalls is neglected. A corresponding averaging of the momentum equations gives

$$\begin{aligned}&\frac{\partial}{\partial x^*}\int_{S^*(x^*,y^*)}^{h^*(x^*,y^*)} \rho^* u^{*2}\,\mathrm{d}z^* + \frac{\partial}{\partial y^*}\int_{S^*(x^*)}^{h^*(x^*,y^*)} \rho^* u^* v^*\,\mathrm{d}z^* + \rho^* g\big(h^* - S^*\big)\frac{\partial h^*}{\partial x^*}\\ &\quad = \rho^* u^{*2}\left.\frac{\partial S^*}{\partial x^*}\right|_{S^*(x^*)} - \mu\left.\frac{\partial u^*}{\partial z^*}\right|_{S^*(x)} - F_x,\end{aligned} \tag{2.2a}$$

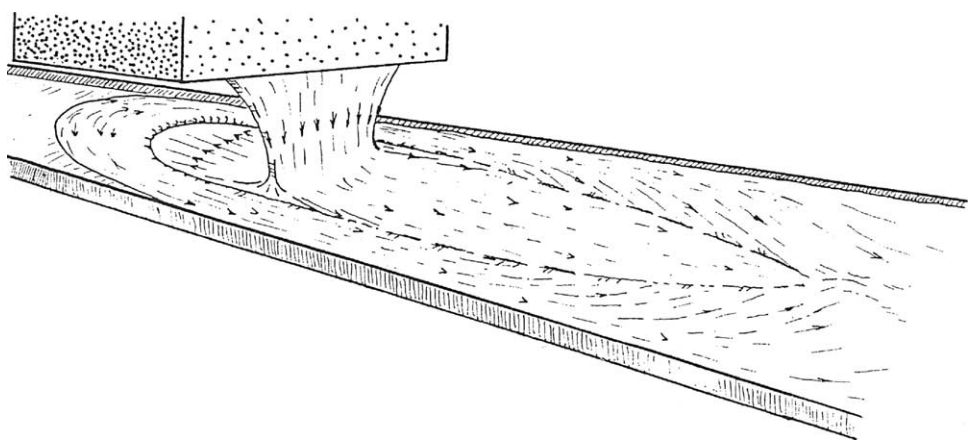

Fig. 1. Schematic view of the flow region.

$$\frac{\partial}{\partial x^*}\int_{S^*(x^*)}^{h^*(x^*,y^*)}\rho^* u^* v^*\,\mathrm{d}z^* + \frac{\partial}{\partial y^*}\int_{S^*(x^*)}^{h^*(x^*,y^*)}\rho^* v^{*2}\,\mathrm{d}z^* + \rho^* g\big(h^* - S^*\big)\frac{\partial h^*}{\partial y^*} = -\mu\frac{\partial v^*}{\partial z^*}\bigg|_{S^*(x^*)} - F_y. \tag{2.2b}$$

Here F_x and F_y are the components of the electromagnetic force $\mathbf{j}\times\mathbf{B}$, caused by the currents induced by the moving fluid and the applied magnetic field.

After averaging there are three independent variables, the liquid thickness $h^*(x^*, y^*)$ and the velocity field

$$\mathbf{U}^* = U^*(x^*, y^*)\mathbf{e}_x + V^*(x^*, y^*)\mathbf{e}_y. \tag{2.3}$$

To proceed, it is convenient to introduce dimensionless variables, so we let

$$U = \frac{U^*}{U_0}, \qquad V = \frac{V^*}{U_0}, \qquad \beta = \frac{V_{\text{belt}}}{U_0}, \tag{2.4}$$

where U_0 is the speed of the impinging jet and V_{belt} is the velocity of the belt.

We normalize all lengths in units of a^*, the thickness of that part of the jet which is initially spread in the casting direction. This means that we let

$$x = \frac{x^*}{a^*}, \qquad y = \frac{y^*}{a^*}, \qquad z = \frac{z^*}{a^*}. \tag{2.5}$$

We also introduce the dimensionless liquid layer thickness $\tilde{h}$ and a dimensionless thickness of the solidified strip $S(x)$ according to

$$\begin{aligned}\tilde{h}(x, y) &= \frac{h^*(x^*, y^*) - S^*(x^*)}{a^*},\\ S(x) &= \frac{S^*(x^*)}{a^*}.\end{aligned} \tag{2.6}$$

The applied magnetic field $\mathbf{B}^*(x^*)$ is normalized to the maximum magnetic field B_0, i.e.,

$$b_0(x) = \frac{B^*(x^*)}{B_0}. \tag{2.7}$$

The components of the induced electric field are scaled as

$$E_x = \frac{E_x^*}{U_0 B_0}, \qquad E_y = \frac{E_y^*}{U_0 B_0}. \tag{2.8}$$

Rewriting the equation of motion in dimensionless form the following dimensionless variables appears. The Reynolds-number R, the Hartmann-number M^2, the Froude-number F^2 and the dimensionless speed of the belt β defined as

$$R = \frac{U_0 a^*}{\nu}, \qquad M^2 = \frac{B_0^2\sigma^* a^{*2}}{\rho\nu}, \qquad F^2 = \frac{U_0^2}{g a^*}, \qquad \beta = \frac{V_{\text{belt}}}{U_0}. \tag{2.9}$$

Another important dimensionless number is the interaction number defined as

$$N = \frac{B_0^2\sigma^* a^*}{\rho U_0}. \tag{2.10}$$

Here σ^* is the conductivity of the liquid melt.

We proceed by specifying the velocity distribution, as a function of the depth. The chosen velocity distribution must fulfill the boundary conditions at the solidification front $S(x)$ and at the free surface $\tilde{h}(x, y)$. Earlier studies of the boundary layer equations for the two-dimensional case show that for the case of a relatively weak magnetic field an initially thin boundary layer in a short distance grows up to the free surface and becomes fully developed (Löfgren and Åkerstedt [5]). The following velocity distribution is then a good approximation for Hartmann-number $M^2 < 5$

$$\begin{aligned}u(x, y, z) &= \frac{3}{2}\big(U(x, y) - \beta\big)\left(\zeta - \frac{1}{3}\zeta^3\right) + \beta,\\ v(x, y, z) &= \frac{3}{2}V(x, y)\left(\varsigma - \frac{1}{3}\zeta^3\right),\\ \zeta &= \frac{z - S(x)}{\tilde{h}(x, y)}.\end{aligned} \tag{2.11}$$

For larger Hartmann numbers $M^2 > 10$ the application of the theory developed in [5] shows a thin Hartmann layer close the moving wall and a velocity distribution of the following type is therefore more appropriate

$$\begin{aligned} u(x,y,z) &= \big(U(x,y)-\beta\big)\big(1-\mathrm{e}^{-M\zeta}\big)+\beta,\\ v(x,y,z) &= V(x,y)\big(1-\mathrm{e}^{-M\zeta}\big),\\ \zeta &= \frac{z-S(x)}{\tilde{h}(x,y)}. \end{aligned} \tag{2.12}$$

We also note the possibility to study turbulent flow by considering a velocity distribution with a sharper derivative close to the wall and in accordance with the empirical laws of a turbulent boundary layer.

Inserting (2.11) or (2.12) into Eqs. (2.1) and (2.2) we get a system of equations, here written, in the conservative form

$$\frac{\partial \mathbf{F}}{\partial x}+\frac{\partial \mathbf{G}}{\partial y}=\mathbf{H}, \tag{2.13}$$

where

$$\mathbf{F}=\left[\tilde{h}(aU+b\beta),\tilde{h}\big(cU^2+d\beta U+e\beta^2\big)+\frac{\tilde{h}^2}{2F^2},\tilde{h}(cU+d/2\beta)V\right]^{\mathrm{T}}, \tag{2.14}$$

$$\mathbf{G}=\left[\tilde{h}aV,\tilde{h}(cU+d/2\beta)V,\tilde{h}cV^2+\frac{\tilde{h}^2}{2F^2}\right]^{\mathrm{T}}. \tag{2.15}$$

The constants $a,\ b,\ c,\ d,\ e$ depend on the particular form of the chosen velocity distribution. For instance for the choice given by (2.11) the values of these constants are $a=5/8,\ b=3/8,\ c=17/35,\ d=39/140,\ e=33/140$.

The source term $\mathbf{H}$ is given by the expressions

$$\begin{aligned} H_1 &= -\beta\frac{\mathrm{d}S}{\mathrm{d}x},\\ H_2 &= -\beta^2\frac{\mathrm{d}S}{\mathrm{d}x}-\frac{1}{F^2}\tilde{h}\frac{\mathrm{d}S}{\mathrm{d}x}-\frac{3(U-\beta)}{2R\tilde{h}}-\frac{M^2}{R}b_0(x)^2a\big(U-E_y(x,y)\big)\tilde{h},\\ H_3 &= -\frac{3V}{2R\tilde{h}}-\frac{M^2}{R}b_0(x)^2a\big(V+E_x(x,y)\big)\tilde{h}. \end{aligned} \tag{2.16}$$

Here the $\mathbf{j}\times\mathbf{B}$-force enters and is written using Ohms law in terms of the electric field and the magnetic field. The explicit form of these fields will be specified later in Section 2.3.

2.2. The growth of the solidified phase

We assume that the liquid metal is fed with no superheat. This gives a considerable simplification of the problem since the growth of the solidified phase can then be solved separately from the fluid flow (Löfgren and Åkerstedt [7]). A simple model for one-dimensional solidification has been suggested by Garcia and Prates [11]. This model cannot be justified strict mathematically, but it gives the correct behavior in two specific limits, the case of ideal solidification and Newtonian cooling solidification. The model also correlates well with experiments. According to this model the position of the solidification front $S(x)$ is given by the expression

$$S(x)=\frac{-S_0+\sqrt{S_0^2+4\alpha\Phi^2x^*/\beta}}{a^*}, \tag{2.17}$$

where the constant S_0 is defined as

$$S_0=\frac{2\alpha\Phi^2\Delta h_f}{h_i(T_f-T_0)}. \tag{2.18}$$

For steel the latent heat of fusion is $\Delta h_f=1.9\times10^9\ \mathrm{J/m^3}$ and the heat diffusion coefficient $\alpha=6\times10^{-6}\ \mathrm{m^2/s}$. h_i is the heat transfer coefficient, which for typical belt strip casting conditions is of the order of 10^4–$10^5\ \mathrm{W/m^2{\cdot}K}$. The temperature difference between the melt and the cooling medium is approximately $T_f-T_0\approx1500$ K. $\Phi\approx1$ is a numerical constant defined in the work by Garcia and Prates [11].

2.3. Transverse magnetic field

After the feeding region a transverse magnetic field in the z-direction is applied. The magnetic field is assumed to increase continuously downstream from zero in the feeding region to a maximum value B_0 for large x. Due to the motion of the melt and the belt a magnetic field is also produced in the casting direction. The size of this magnetic field depends on the magnetic Reynolds number $R_m = \mu_0 U_0 \sigma L$.

Using the thickness of the liquid as the relevant length $L = a^*$ we get a magnetic Reynolds number of the order of 10^{-2}. This means that the induced magnetic field in the direction of the flow is of the order of $R_m B_0$ and is therefore neglected (see Moreau [12]).

The liquid is confined laterally by stationary isolated sidewalls at $y^* = \pm L^*/2$. The dominating flow direction is the x-direction and the velocity field is $\mathbf{u}^*$. The liquid metal is fed onto a conveyor belt made of copper, which moves with the velocity V_{belt} in the casting direction. As the liquid enters the region of an increasing magnetic field, electric fields $\mathbf{E}^*$ and currents $\mathbf{j}^*$ are induced.

These are related via Ohm's law

$$\mathbf{j}^* = \sigma^*\big(\mathbf{E}^* + \mathbf{u}^* \times \mathbf{B}^*\big), \tag{2.19}$$

where σ^* is the conductivity of the medium. Since the electric field is conservative we use the electrostatic potential ϕ^*

$$\mathbf{E}^* = -\nabla\phi^*. \tag{2.20}$$

Considering a steady current, we have from the conservation of charge

$$\nabla \cdot \mathbf{j}^* = 0. \tag{2.21}$$

Together with Ohm's law (2.19) we get

$$\nabla \cdot \big(\sigma^* \nabla\phi^*\big) = \nabla \cdot \big(\sigma^* \mathbf{u}^* \times \mathbf{B}^*\big). \tag{2.22}$$

Introducing Cartesian coordinates, this gives

$$\sigma^* \frac{\partial^2\phi^*}{\partial x^{*2}} + \sigma^* \frac{\partial^2\phi^*}{\partial y^{*2}} + \frac{\partial}{\partial z^*}\left(\sigma^* \frac{\partial\phi^*}{\partial z^*}\right) = \frac{\partial}{\partial x^*}\big(\sigma^* v^* B^*\big) - \frac{\partial}{\partial y^*}\big(\sigma^* u^* B^*\big). \tag{2.23}$$

The conductivity is assumed to be a piecewise constant function of z. Let σ_2^* be the conductivity of the liquid metal and the solidified strip and σ_1^* the conductivity of the copper belt.

In order to perform a multiple length scale analysis, we introduce the following dimensionless variables

$$\eta = \frac{z+\delta}{\tilde{h}(X,Y) + S(X) + \delta}, \quad X = \frac{x}{L}, \quad Y = \frac{y}{L}, \quad \bar{h} = \frac{\tilde{h}(X,Y) + S(X) + \delta}{L}, \tag{2.24}$$

where δ is the thickness of the copper belt, $S(X)$ the thickness of the solidified strip and L the width of the copper belt, all normalized to a^*.

Since the liquid layer is considered thin, we adopt a multiple length scale analysis treating the vertical coordinate η as a fast variable and X and Y as slow variables.

We also introduce a dimensionless potential $\bar{\phi}$ according to

$$\phi^*\big(x(X), y(Y), z(X,Y,\eta)\big) = U_0 B_0 L a^* \bar{\phi}(X,Y,\eta), \tag{2.25}$$

and dimensionless velocities and magnetic field according to

$$u = \frac{u^*}{U_0}, \qquad v = \frac{v^*}{U_0}, \qquad b_0(X) = \frac{B^*(X)}{B_0}. \tag{2.26}$$

We also define a dimensionless conductivity σ defined as

$$\sigma = \frac{\sigma^*}{\sigma_1^*}, \tag{2.27}$$

where σ_1^* is the conductivity of the belt.

Eq. (2.23) rewritten in these variables then becomes

$$\begin{aligned}
&\frac{\partial}{\partial\eta}\left(\sigma\frac{\partial\bar{\phi}}{\partial\eta}\right) + \bar{h}^2\sigma\left(\frac{\partial^2\bar{\phi}}{\partial X^2} + \frac{\partial^2\bar{\phi}}{\partial Y^2}\right) - \bar{h}^2\sigma\left(2\eta\frac{\bar{h}_X}{\bar{h}}\frac{\partial^2\bar{\phi}}{\partial X\partial\eta} - \eta\left(2\left(\frac{\bar{h}_X}{\bar{h}}\right)^2 + 2\left(\frac{\bar{h}_Y}{\bar{h}}\right)^2 - \frac{\bar{h}_{XX}}{\bar{h}} - \frac{\bar{h}_{YY}}{\bar{h}}\right)\frac{\partial\bar{\phi}}{\partial\eta}\right.\\
&\quad\left. - \eta^2\left(\left(\frac{\bar{h}_X}{\bar{h}}\right)^2 + \left(\frac{\bar{h}_Y}{\bar{h}}\right)^2\right)\frac{\partial^2\bar{\phi}}{\partial\eta^2} + 2\eta\frac{\bar{h}_Y}{\bar{h}}\frac{\partial^2\bar{\phi}}{\partial Y\partial\eta}\right) = \sigma\bar{h}^2\left(\frac{\partial(b_0(X)v)}{\partial X} - \frac{\partial(b_0(X)u)}{\partial Y}\right).
\end{aligned} \tag{2.28}$$

Next we assume the liquid layer to be thin, i.e., we put

$$\bar{h} \ll 1. \tag{2.29}$$

Assuming an expansion in powers of $\bar{h}^2$ for the potential

$$\bar{\phi} = \phi_0 + \bar{h}^2\phi_1 + \mathrm{O}(\bar{h}^4), \tag{2.30}$$

and putting this expansion into (2.28) we get to zero order

$$\frac{\partial}{\partial\eta}\left(\sigma\frac{\partial\phi_0}{\partial\eta}\right) = 0. \tag{2.31}$$

With the solution

$$\sigma\frac{\partial\phi_0}{\partial\eta} = g(X, Y), \tag{2.32}$$

where g is an arbitrary function of X and Y.

At the bottom of the belt ($\eta = 0$) and at the free surface of the liquid ($\eta = 1$), there are no normal components of the electric current. Therefore

$$\left.\frac{\partial\phi_0}{\partial\eta}\right|_{\eta=0,1} = 0, \tag{2.33}$$

from which it follows that the zero order potential can only be a function of X and Y. To the next order we get

$$\frac{\partial}{\partial\eta}\left(\sigma\frac{\partial\phi_1}{\partial\eta}\right) + \sigma\left(\frac{\partial^2\phi_0}{\partial X^2} + \frac{\partial^2\phi_0}{\partial Y^2}\right) = \sigma\left(\frac{\partial(b_0(X)v)}{\partial X} - \frac{\partial(b_0(X)u)}{\partial Y}\right). \tag{2.34}$$

To determine the zero order potential we use a solvability condition, which can be found by integrating Eq. (2.34) from 0 to 1, using the boundary conditions (2.33). The solvability condition becomes

$$\int_0^1 \sigma\left(\frac{\partial^2\phi_0}{\partial X^2} + \frac{\partial^2\phi_0}{\partial Y^2}\right)\mathrm{d}\eta = \int_0^1 \sigma\left(\frac{\partial(b_0(X)\mathrm{v})}{\partial X} - \frac{\partial(b_0(X)u)}{\partial Y}\right)\mathrm{d}\eta. \tag{2.35}$$

Note that the contribution to the right-hand side of (2.35) from the belt and the solidified strip is zero.

Evaluating (2.35) we get

$$\frac{\partial^2\phi_0}{\partial X^2} + \frac{\partial^2\phi_0}{\partial Y^2} = \frac{\sigma_2(\delta + S + \tilde{h})}{(\sigma_1\delta + \sigma_2 S + \sigma_2\tilde{h})} \int_{(\delta+\tilde{\Delta})/(\delta+\Delta+\tilde{h})}^1 \left(\frac{\partial(b_0(X)v)}{\partial X} - \frac{\partial(b_0(X)u)}{\partial Y}\right)\mathrm{d}\eta. \tag{2.36}$$

The conductivity of the copper belt σ_1 is typically two orders of magnitude larger than the conductivity σ_2 of the liquid and the strip. Therefore, when the integrand is finite, the right-hand side of (2.36) can be neglected and we find an approximate equation for the zero order potential in the form

$$\frac{\partial^2\phi_0}{\partial X^2} + \frac{\partial^2\phi_0}{\partial Y^2} = 0. \tag{2.37}$$

This potential equation (2.37) is a considerable simplification when compared with the exact equation (2.28). Especially since the potential to lowest order is independent of the flow field. Within this approximation we note that the electric field is the same in the belt, the strip and in the liquid.

We assume that the liquid metal enters into the region where the magnetic field is zero. Downstream the magnetic field then grows continuously from zero to a maximum value B_0. Explicitly, we assume a magnetic field distribution according to the expression

$$b_0(X) = \frac{1}{2}\big(1 + \mathrm{erf}\big(\gamma(X - X_0)\big)\big). \tag{2.38}$$

Here γ^{-1} is the scale of the spatial variation of the magnetic field and X_0 is the position where the magnitude of the magnetic field has grown to half of its maximum value.

As the liquid enters this region, an electric field is induced, which can be calculated by solving Eq. (2.37) supplemented with appropriate boundary conditions.

The sidewalls are assumed to be stationary isolators. The boundary condition consistent with the approximation (2.37) for the potential ϕ_0 can therefore be determined from the condition that the y-component of the current averaged over the thickness must be zero at the walls. The appropriate boundary conditions are therefore

$$\left.\frac{\partial\phi_0}{\partial Y}\right|_{Y=\pm1/2} = -\beta b_0(X) \tag{2.39}$$

and

$$\phi_0 \to -\beta Y b_0(X) \quad \text{as } X \to \infty$$

and

$$\phi_0 \to 0 \quad \text{as } X \to -\infty. \tag{2.40}$$

The solution of this potential problem is given by

$$\begin{aligned}\phi_0(X,Y) = -\beta b_0(X)Y + \sum_{n=1,3,5,\ldots}^{\infty} \frac{\beta}{n^2\pi^2}\Bigg\{ & \mathrm{e}^{-\frac{1}{4}n\pi(4\gamma^2(X-X_0)-n\pi)/\gamma^2}\left(1+\operatorname{erf}\left(\frac{1}{2}\frac{2\gamma^2(X-X_0)-n\pi}{\gamma}\right)\right) \\ & + \mathrm{e}^{\frac{1}{4}n\pi(4\gamma^2(X-X_0)+n\pi)/\gamma^2}\left(\operatorname{erf}\left(\frac{1}{2}\frac{2\gamma^2(X-X_0)+n\pi}{\gamma}\right)-1\right)\Bigg\}\cos\left(n\pi\left(Y+\frac{1}{2}\right)\right).\end{aligned} \tag{2.41}$$

The electric field is therefore divided into two parts. A transient electric field with components in the x and y-directions, which appears at the entrance of the magnetic field region, and vanishes for large x and an electric field $\beta b_0(X)$ in the y-direction, which approaches the constant value β for large x. The transient part of the electric field gives currents, which are closed in the $x-y$-plane (see Shercliff [13]). The y-component of the current due to the non-transient electric field $\beta b_0(X)$ is given by $\sigma b_0(X)(\beta-u)$, where u is the velocity of the liquid or the velocity of the belt and the strip, the latter two both equal to β. Within this approximation we then have $\sigma b_0(X)(\beta-u)=0$ in the strip and belt. This means that it is not clear how this part of the current is closed. In order to find how the current closes the finite conductivity of the strip and belt must be taken into account. It is reasonable that this part of the current is closed in a boundary layer close to the sidewalls. Therefore we introduce the stretched boundary layer coordinate Y^*

$$Y^* = \frac{Y-1/2}{\bar{h}(X,Y)^{\nu}}. \tag{2.42}$$

Introducing this variable into the equation for the potential (2.28) we find the value of ν to be 1, corresponding to a boundary layer thickness of order $\mathrm{O}(\bar{h})$. The leading order boundary layer equation then becomes

$$\frac{\partial}{\partial\eta}\left(\sigma\frac{\partial\phi^i}{\partial\eta}\right)+\sigma\frac{\partial^2\phi^i}{\partial Y^{*2}}=0. \tag{2.43}$$

Using the method of separation of variables we find the following solution for the boundary layer equation

$$\phi^i = -\alpha\beta b_0(X)C_0Y^* + \sum_{n=1}^{\infty} C_n\,\mathrm{e}^{k_nY^*}g_n(\eta) + C_0', \tag{2.44}$$

where $\alpha,\ C_n,\ C_0, C_0'$ are constants. The eigenfunctions $g_n(\eta)$ are determined from the following eigenvalue problem

$$\begin{aligned}&\frac{\mathrm{d}^2g_n}{\mathrm{d}\eta^2}+k_n^2g_n=0,\\ &g_n'(\eta)=0 \quad \text{at } \eta=0 \text{ and } \eta=1,\\ &g_n\big(\bar{\delta}+\big)-g_n\big(\bar{\delta}-\big)=\frac{\tau\sigma_2^*}{a^*(\delta+S(X)+\tilde{h}(X,1/2))}g_n'\big(\bar{\delta}+\big),\\ &\sigma_1g_n'\big(\bar{\delta}-\big)=\sigma_2g_n'\big(\bar{\delta}+\big),\end{aligned} \tag{2.45}$$

where

$$\bar{\delta}=\frac{\delta}{\delta+S+\tilde{h}}. \tag{2.46}$$

The second boundary condition originates from the assumption of a non-perfect contact between the solidified strip and the belt, where the contact resistance τ is introduced.

In a direct strip casting application the contact between the strip and belt may not be perfect, but the actual numerical value of the contact resistance is not known. The other two boundary conditions correspond to no normal current at the liquid surface and the bottom of the belt and continuity of the normal current at the strip-belt interface.

The eigenvalue problem (2.45) gives the eigenvalues k as solutions of the equation

$$\frac{\sigma_2}{\sigma_1}\cos(k\bar{\delta})\sin\big(k(1-\bar{\delta})\big)+\sin(k\bar{\delta})\big\{\cos\big(k(1-\bar{\delta})\big)-Tk\sin\big(k(1-\bar{\delta})\big)\big\}=0, \tag{2.47}$$

where $T=\tau\sigma_2^*/(a^*(\delta+S(X)+\tilde{h}(X,1/2)))$ is a dimensionless quantity related to the contact resistance. The eigenfunctions are orthogonal over the interval with respect to the weight function σ and the eigenvalue problem is self-adjoint. Note that the weight function is equal to the dimensionless conductivity.

To determine the constants we first need to match the boundary layer solution with the outer non-transient solution which in the limit of large conductivity of the belt is given by $-\beta b_0(X)Y+\mathrm{O}(\sigma_2/\sigma_1)$.

Matching gives

$$\phi^i=-\alpha\beta b_0(X)\left(\bar{h}\left(X,\frac{1}{2}\right)Y^*+\frac{1}{2}\right)+\sum_{n=1}^{\infty}C_n\,\mathrm{e}^{k_nY^*}g_n(\eta), \tag{2.48}$$

where the leading order value of α in an expansion in powers of σ_2/σ_1 is equal to one.

Next, we impose a boundary condition for the y-component of the current. Since the sidewalls are isolated the y-component of the current must be zero at the walls. The boundary condition at $Y^*=0$ is therefore

$$j_y\Big|_{Y^*=0}=-\sigma\frac{\partial\phi^i}{\partial Y}\Big|_{Y^*=0}-\sigma u\left(X,\frac{1}{2},\eta\right)b_0(X)=0, \tag{2.49}$$

imposed in the belt, strip and liquid and where $\sigma=\sigma^*/\sigma_1^*$.

Inserting (2.48) into (2.49) and multiplying by the eigenfunction $g_0(\eta)=1$ and integrating from zero to one, we find the following expression for the constant α

$$\alpha=\frac{\sigma_1\delta\beta+\sigma_2S\beta+\sigma_2\bar{u}\tilde{h}}{\sigma_1\delta\beta+\sigma_2S\beta+\sigma_2\beta\tilde{h}}, \tag{2.50}$$

where $\bar{u}$ is the average value of $u(X,1/2,\eta)$ over the liquid phase, which for the choice of velocity distribution given by for instance (2.12) becomes $aU+b\beta$, where U is the velocity of the free surface and a and b are given by

$$a=1-M^{-1}+M^{-1}\exp(-M),\qquad b=M^{-1}-M^{-1}\exp(-M). \tag{2.51}$$

The constants C_n are determined from multiplying (2.49) by $g_m(\eta)$ and integrating, which gives

$$C_m=-\bar{h}\left(X,\frac{1}{2}\right)\frac{b_0(X)}{k_m}\frac{\int_0^1\sigma u(X,1/2,\eta)g_m(\eta)\,\mathrm{d}\eta}{\int_0^1\sigma g_m(\eta)^2\,\mathrm{d}\eta}. \tag{2.52}$$

The potential in the boundary layer region is therefore

$$\phi^i\big(X,Y^*,\eta\big)=-\frac{\sigma_1\delta\beta+\sigma_2S\beta+\sigma_2\bar{u}\tilde{h}}{\sigma_1\delta\beta+\sigma_2S\beta+\sigma_2\beta\tilde{h}}\beta b_0(X)\left(\bar{h}\left(X,\frac{1}{2}\right)Y^*-\frac{1}{2}\right)+\sum_{n=1}^{\infty}C_n\,\mathrm{e}^{k_nY^*}g_n(\eta). \tag{2.53}$$

Expanding (2.53) in the limit of large conductivity of the belt we find for the first term

$$\phi^i(X,Y,\eta)=-\left(1+\frac{a\tilde{h}(U-\beta)}{\beta\delta}\frac{\sigma_2}{\sigma_1}+\mathrm{O}\left(\left(\frac{\sigma_2}{\sigma_1}\right)^2\right)\beta b_0(X)Y+\cdots\right), \tag{2.54}$$

where the constant a depends upon the particular velocity distribution. We note that the first term in an expansion in powers of σ_2/σ_1 agrees with the outer solution given by (2.41). The y-component of the currents in the belt, strip and liquid are then respectively

$$\begin{aligned}
j_y&=\sigma_1\left(\frac{a\tilde{h}(U-\beta)}{\beta\delta}\frac{\sigma_2}{\sigma_1}\right)\beta b_0(X)+\cdots,\\
j_y&=\sigma_2\left(\frac{a\tilde{h}(U-\beta)}{\beta\delta}\frac{\sigma_2}{\sigma_1}\right)\beta b_0(X)+\cdots,\\
j_y&=\sigma_2\left(\left(1+\frac{a\tilde{h}(U-\beta)}{\beta\delta}\frac{\sigma_2}{\sigma_1}\right)\beta-u\left(X,\frac{1}{2},\eta\right)\right)b_0(X)+\cdots.
\end{aligned} \tag{2.55}$$

These expressions reveal the distribution of the y-component of the current in the different phases. It also shows that if we are only interested in the current in the liquid phase in the limit of small σ_2/σ_1 it is a reasonable approximation to keep only the leading order term. The current in the z-direction is only different from zero in the boundary layer and can be calculated from (2.53). This current however does not give any contribution to the $\mathbf{j} \times \mathbf{B}$ force in the liquid.

To see more clearly how the currents close in the boundary layer near a sidewall, we have plotted the current vector field in Fig. 3. The vector field is calculated from Eq. (2.53) with the value of $T = 50$ and with the belt/solid interface at $\eta = 0.3$ and the solid/liquid interface at $\eta = 0.5$.

The combined effect of the electric field and the magnetic field gives a braking action of the liquid metal flow. This action continues until the final favorable state corresponding to uniform velocity and constant thickness is reached. In this asymptotic limit the braking force becomes zero.

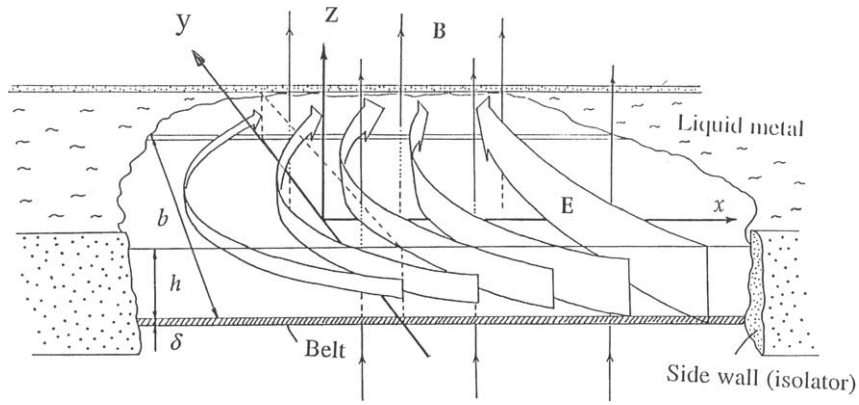

Fig. 2. The entrance into the magnetic field region with induced currents.

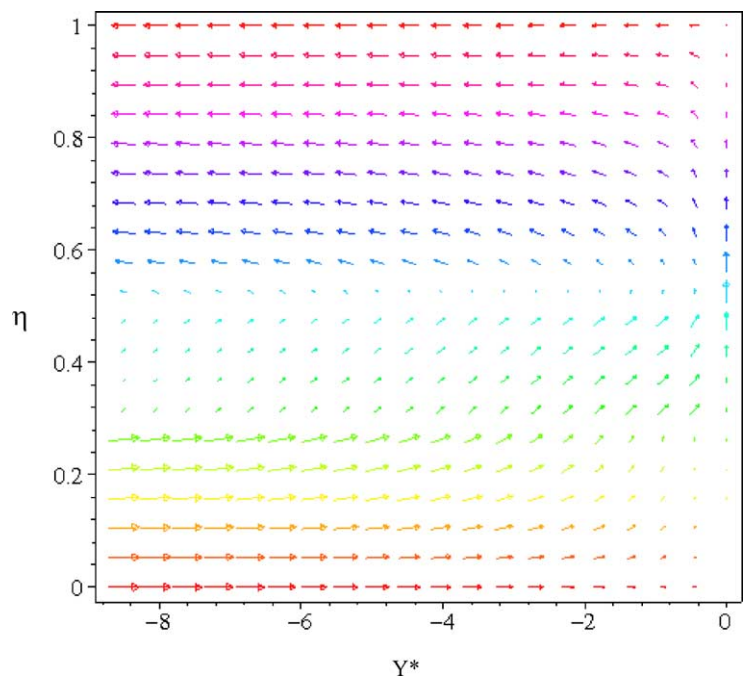

Fig. 3. The distribution of current in the boundary layer region close to the sidewall ($Y^* = 0$) for the parameters $T = 50$, $\sigma_2/\sigma_1 = 0.01$. The belt/solid interface is at $\eta = 0.3$ and the solid/liquid interface at $\eta = 0.5$.

2.4. Supercritical flow

For mathematical classification of the system (2.13) we write it in terms of primitive variables $\mathbf{q} = [\tilde{h} \quad U \quad V]^{\mathrm{T}}$. The system then becomes

$$\mathbf{B}\frac{\partial \mathbf{q}}{\partial x} + \mathbf{C}\frac{\partial \mathbf{q}}{\partial y} = \mathbf{H}, \tag{2.56}$$

where the matrices $\mathbf{B}$ and $\mathbf{C}$ are given by

$$\mathbf{B} = \begin{bmatrix} aU + b\beta & a\tilde{h} & 0 \\ cU^2 + dU\beta + e\beta^2 + \frac{\tilde{h}}{F^2} & \tilde{h}(2cU + d\beta) & 0 \\ cUV + \frac{d}{2}\beta V & \tilde{h}cV & \tilde{h}\left(cU + \frac{d}{2}\beta\right) \end{bmatrix}, \tag{2.57}$$

$$\mathbf{C} = \begin{bmatrix} aV & 0 & a\tilde{h} \\ cUV + \frac{d}{2}\beta V & \tilde{h}cV & \tilde{h}\left(cU + \frac{d}{2}\beta\right) \\ cV^2 + \frac{\tilde{h}}{F^2} & 0 & 2\tilde{h}cV \end{bmatrix}. \tag{2.58}$$

The mathematical structure of the system depends on the eigenvalues, i.e., the solutions of the characteristic equation

$$\det(\lambda\mathbf{B} - \mathbf{C}) = 0 \tag{2.59}$$

or

$$\left(\lambda - \frac{V}{U + (d/(2c))\beta}\right)\left(A_1\lambda^2 + 2A_2\lambda + A_3\right) = 0, \tag{2.60}$$

where

$$A_1 = \beta^2(ae - bd) - 2bc\beta U - acU^2 + \frac{a\tilde{h}}{F^2}, \qquad A_2 = c(aU + b\beta)V, \qquad A_3 = \frac{a\tilde{h}}{F^2} - acV^2. \tag{2.61}$$

The choice of a numerical method for the solution of system (2.56) depends to a large degree upon the eigenvalues. For instance if all eigenvalues are real, the system (2.56) is termed hyperbolic and the system can be solved numerically using space marching in the flow direction.

For the special case of zero belt velocity $\beta = 0$ and no source term $\mathbf{H} = 0$ the system is reduced to the ordinary shallow-water equations with the following eigenvalues

$$\lambda_1 = \frac{U}{V}, \qquad \lambda_{2,3} = \frac{UV}{U^2 - h/F^2} \pm \frac{\sqrt{h/F^2(U^2 + V^2 - h/F^2)}}{U^2 - h/F^2}. \tag{2.62}$$

All eigenvalues are real if

$$\frac{U^2 + V^2}{h/F^2} > 1. \tag{2.63}$$

The equation system is then hyperbolic and the flow is called supercritical if

$$\frac{U^2 + V^2}{h/F^2} < 1, \tag{2.64}$$

two eigenvalues are complex and the flow is called subcritical. In the same way we classify the flow (2.56) as supercritical if all eigenvalues are real.

Previous studies of the two-dimensional flow [5] show that no plane hydraulic jumps can form if the following condition is fulfilled

$$\beta > F^{-2/3}, \tag{2.65}$$

i.e., the flow is everywhere supercritical. In the present paper, for the three-dimensional case, we will only consider the case where the flow is supercritical. All the eigenvalues of (2.60) are then real. Even if the condition (2.65) rules out the possibility of plane hydraulic jumps we will see in the following that for the three-dimensional case oblique hydraulic jumps may exist even though (2.65) is fulfilled.

The assumption of supercritical flow gives a lower limit of the belt velocity. To remain supercritical everywhere the belt velocity must be sufficiently large. However in belt strip casting this condition is reasonable, especially for those large production rates, which are needed in a commercial application of the method.

3. Numerical method

The assumption of a supercritical flow means that we may use a space marching numerical method. The system of equations is then hyperbolic and for such problems there are efficient modern numerical methods, which automatically takes care of discontinuities such as shocks in compressible fluids and hydraulic jumps in shallow-water models, see Toro [14] and LeVeque [15]. In the present work we use a development of a method originally suggested by Roe [16] for a numerical treatment of Eulers equations. Glaister [17] developed this method further for the application to shallow water flows. One disadvantage of the method given by Roe is that it may generate unphysical expansion shocks (jumps). This undesirable feature of the method can however be cured by introducing the concept of an entropy fix [14,15].

In the present work the source terms are of large importance and several methods have been suggested for their treatment. The simplest method is to use fractional step splitting (or x-splitting in the present application). In this method one uses a fractional step procedure in which one first solves the homogenous problem with no source terms, and secondly advances the solution forward in time (here in x) by assuming no variation in space (here in y). This method has been shown to be unsatisfactory especially in treating shallow water flows with geometric source terms, such as bed elevation. Here in the present application this corresponds to the growing solidified phase beneath the liquid.

Methods based on up-winding the source term [18–20] have been shown to resolve these difficulties and therefore this is the method applied in the present paper. The development of improved numerical methods in treating source terms is at present investigated by several researchers.

Another disadvantage of the approximate Riemann solver by Roe, when compared with an exact Riemann solver is that although the shocks (oblique jumps) are resolved quite well using the method by Roe, the resolution of the slip lines is poor. Across a slip line (or tangential discontinuity) the velocity may jump abruptly while the liquid layer thickness is the same. A method which gives excellent slip lines for steady supercritical shallow water flow with no source terms has been developed by Yang et al. [21]. However to the authors knowledge no method has been developed which can achieve good resolution of slip lines together with a treatment of source terms. At the present stage of this work we therefore find it sufficient to consider the approximate Riemann solver by Roe in combination with using the method of up winding the source terms. In the next section we present some results showing the resolution of the slip lines using this method. It will be seen that in the method considered slip lines are resolved to some extent, but not as good as for the jumps. Some details of the development of the approximate Riemann solver by Roe to the present application are given in Appendix.

4. Numerical results

In the present paper we consider results corresponding to the case of feeding the liquid metal through a slit or down an inclined plane. The slit then generates a finite plane jet, falling vertically onto the belt. Using an inclined plane the jet is falling obliquely onto the belt. The initial conditions for the flow downstream of the jet are however not known in detail. These conditions depend on details of the flow in the plane 3D jet, which are not known and require a separate numerical treatment. From the studies of the two-dimensional case the exact details of the jet flow are however not very decisive for the subsequent flow. We therefore believe that choosing initial conditions for the three-dimensional case capturing only the gross features of the jet flow is sufficient for the description of the flow downstream of the jet.

We present results for two different feeding conditions. In the first case we consider a vertically falling flat jet of finite width in the y-direction equal to 100 units of a^*.

Approximately half of the jet will flow against the casting direction, and is limited upstream by a meniscus. This liquid will flow around the edges of the jet and later becomes an outer part of the main flow in the casting direction. A center part with large velocity and shallow depth and an outer part with a slower velocity and larger depth then characterize the flow in the casting direction. According to simple experiments with water the outer part has a velocity close to belt velocity. As initial conditions we therefore choose an inner region with shallow depth and large velocity corresponding to the jet directly spread in the casting direction, and an outer part with velocity equal to the belt velocity and a larger depth, originating from the back flow. An idealized discontinuity in depth and velocity is chosen to separate the two regions.

We present the results as free surface level distributions $h(x, y)$ as functions of x and y and some results concerning the distribution of the local Froude number $(U^2 + V^2)/\tilde{h}$.

In the first example we consider the case with no magnetic field ($M^2 = 0$) and no solidification. The values of the dimensionless parameters are chosen as $R = 4500$, $F^2 = 32$, $\beta = 0.4$. (This corresponds for instance to a jet velocity of $U_0 = 1.1$ m/s and a jet thickness of 8 mm.) The solution for this case is shown in Fig. 4. In the figure we note the typical pattern of oblique hydraulic jumps, which occurs due to the propagation of the discontinuity in the initial conditions. The jumps are reflected at the sidewalls and a standing wave pattern is formed. This pattern is only weakly damped downstream by viscous dissipation. This kind of oblique hydraulic jump pattern is also seen in open water channels. For instance if the water levels in

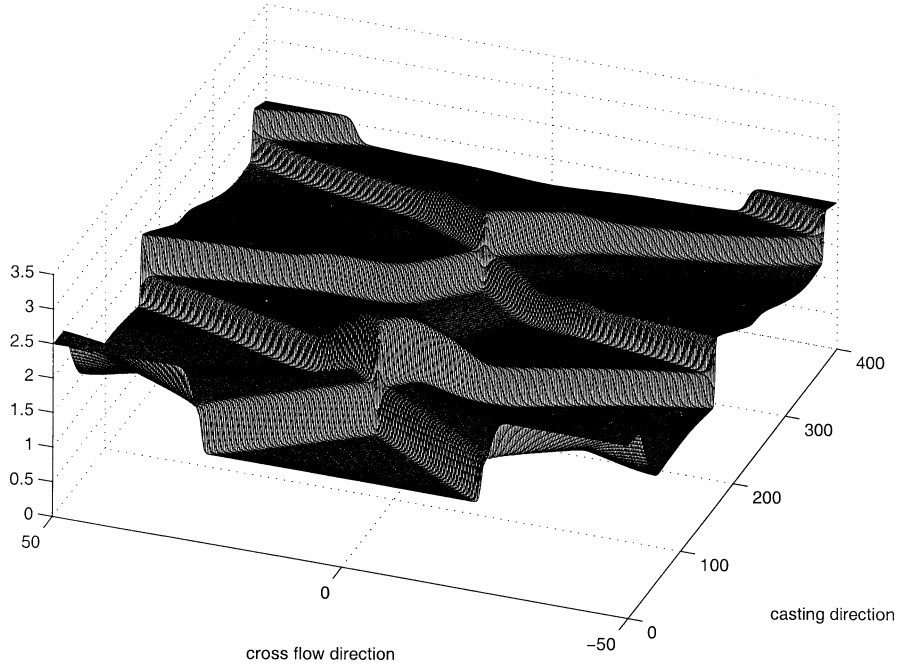

Fig. 4. Free-surface level distribution $h(x, y)$ without magnetic field and no solidification. Parameters $R = 4500,\ F^2 = 32,\ \beta = 0.4,\ M^2 = 0$.

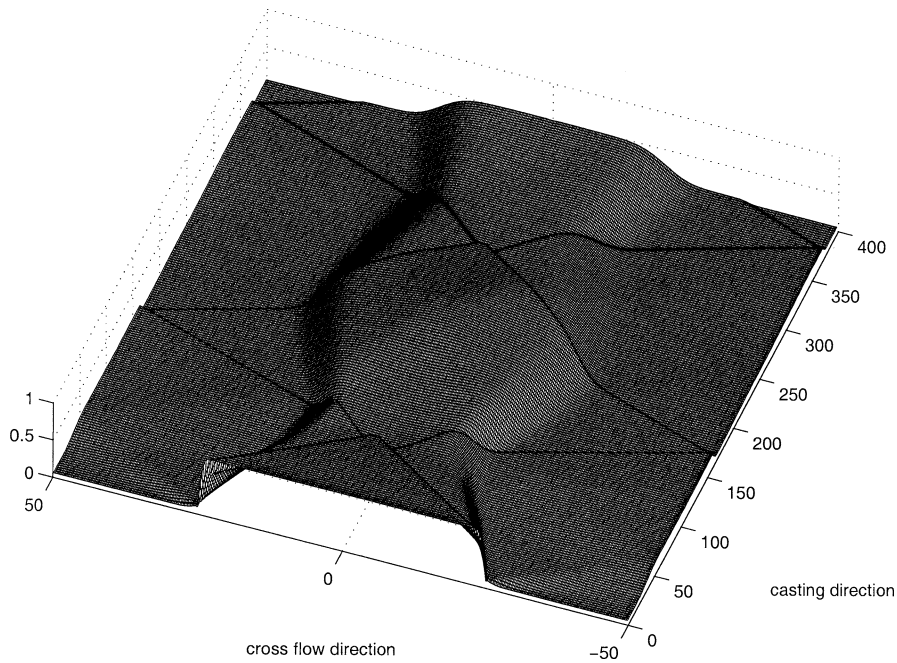

Fig. 5. The local Froude-number $(U^2 + V^2)/\tilde{h}$ distribution with parameters $R = 4500,\ F^2 = 32,\ \beta = 0.4,\ M^2 = 0$ and no solidification.

two sections of a channel are different, separated by sluice gate, and if the sluice is slightly raised, reflecting oblique hydraulic jumps are seen downstream of the gate as long as the water level is sufficiently small for the flow to stay supercritical.

Due to the very weak viscous damping, the braking length, i.e., the distance to reach the final state of uniform velocity and a smooth horizontal surface is very long. This result is in agreement with the results of our previous two-dimensional theory [4].

In Fig. 5 the local Froude number $(U^2 + V^2)/\tilde{h}$ is presented as a function of x and y.

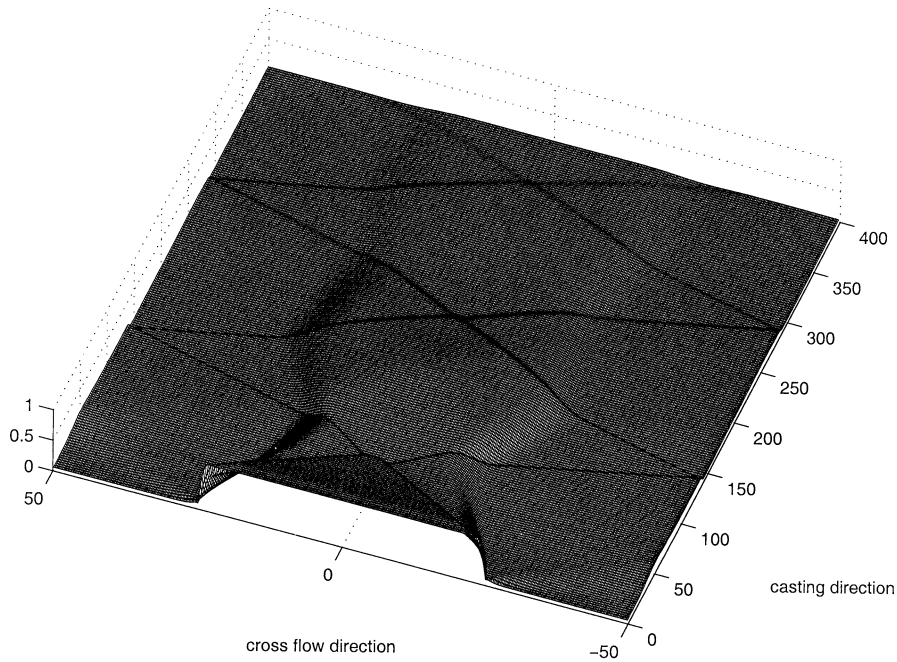

Fig. 6. The local Froude-number $(U^2 + V^2)/\tilde{h}$ distribution with the parameters $M^2 = 20$, $R = 4500$, $F^2 = 32$ and no solidification.

As discussed earlier there are ideally two kinds of discontinuities for this variable. We have the discontinuity corresponding to the jump in surface level and the slip-lines discontinuity corresponding to a jump in velocity. We can see that the oblique jump discontinuities are well resolved whereas the slip-lines are initially resolved but smear out downstream.

In Fig. 6 the distribution of the local Froude number is shown corresponding to the case of a flow without solidification and a magnetic field with Hartman-number $M^2 = 20.0$ ($B = 0.11$ T). The scale length of the applied magnetic field is chosen such that the field grows smoothly from zero up to its maximum in a distance of $20a^*$. Here we note that the slip lines can only be identified initially.

It is known [12,13] that at the entrance into a region of transverse magnetic field, vorticity is created, so that an M-shaped velocity profile may occur. For the present case this effect may be estimated by taking the curl of Eulers equation, so that

$$\rho^*(\mathbf{u}^* \cdot \nabla)\boldsymbol{\omega} = (\mathbf{B}_0 \cdot \nabla)\mathbf{j}^* - (\mathbf{j}^* \cdot \nabla)\mathbf{B}_0. \tag{4.1}$$

An estimate of the order of magnitude of these terms gives

$$\frac{\partial U}{\partial Y} \approx \frac{\sigma^* B_0^2 a^* L}{\rho U_0} \frac{\partial \bar{\phi}}{\partial X}, \tag{4.2}$$

where $\partial\bar{\phi}/\partial X$ is given by (2.41) and $\partial U/\partial Y$ is the approximate vorticity generated. Solving for U we get the velocity at the side wall as

$$U \approx \frac{\sigma B_0^2 a^* L}{\rho U_0} \int_0^{1/2} \frac{\partial \bar{\phi}}{\partial X}\,\mathrm{d}Y = NL \int_0^{1/2} \frac{\partial \bar{\phi}}{\partial X}\,\mathrm{d}Y. \tag{4.3}$$

Numerical integration of the integral gives the value 0.06. With typical numbers the modified velocity becomes small of the order of 0.012. So in the present application with rather weak magnetic fields this effect of jetting at the sidewalls is very small.

Fig. 7 shows the x-component of the free surface velocity U for $M^2 = 0$ as function of Y for some different positions downstream. This figure should be compared with the same plot presented in Fig. 8 which shows the corresponding case with a Hartmann number $M^2 = 20$. Comparing the velocity near the sidewall, we find no acceleration due to the vorticity generating mechanism discussed above, and is therefore consistent with the estimate given above. In fact in Fig. 8 we only note the braking mechanism of the electromagnetic force, leading to a slower velocity.

In Fig. 9 the surface level for a flow with solidification but no magnetic field is shown. The growth of the solidified phase is given by Eq. (2.17), with the value of S_0 chosen to be 0.45. This means that the liquid is completely solidified after a

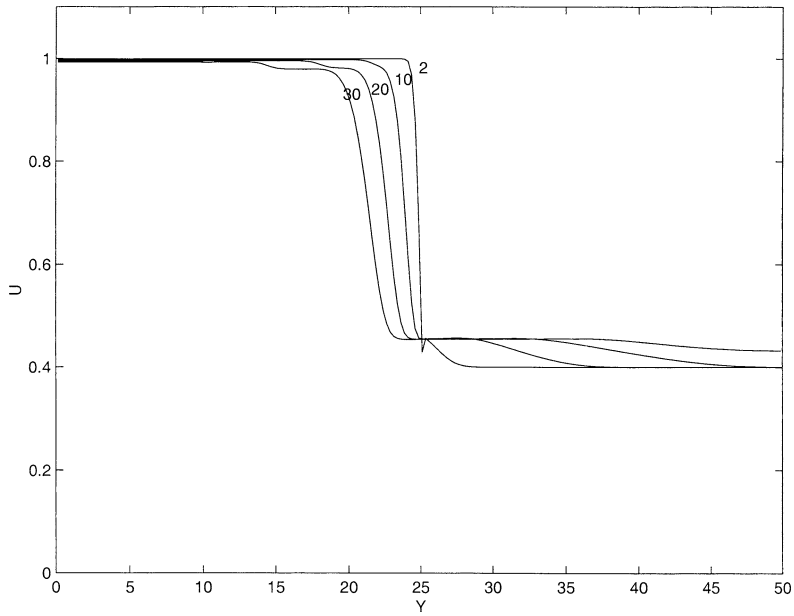

Fig. 7. The free surface velocity as function of Y for different positions downstream $2a^*$, $10a^*$, $20a^*$, $30a^*$ for $R = 4500$, $F^2 = 32$, $\beta = 0.4$, $M^2 = 0$.

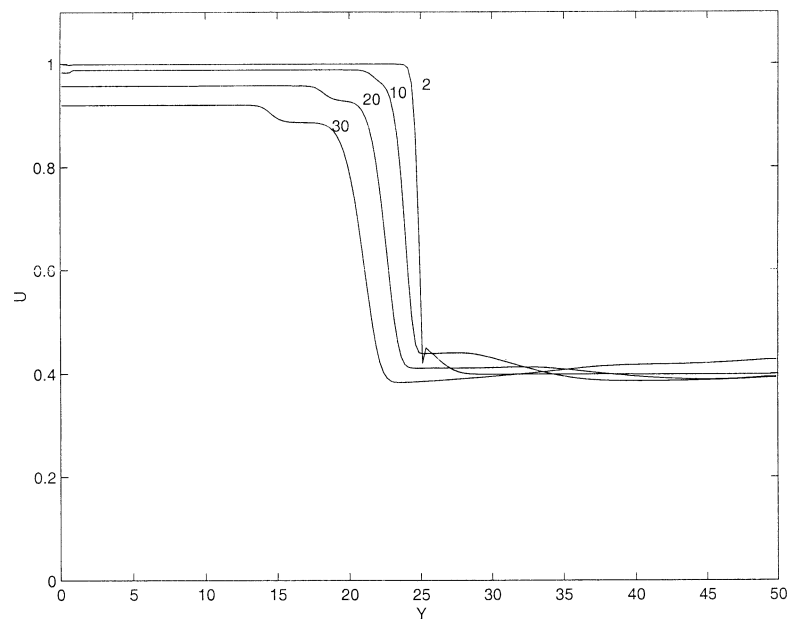

Fig. 8. The free surface velocity as function of Y for different positions downstream $2a^*$, $10a^*$, $20a^*$, $30a^*$ for $R = 4500$, $F^2 = 32$, $\beta = 0.4$, $M^2 = 20$.

length of approximately $600a^*$ (2.4 m with $a^* = 4$ mm). It is seen from Fig. 9 that the steady wave pattern for this case is more damped than for the case with no solidification. The increased damping is due to the effective Reynolds-number, which decreases concurrently with the decreasing thickness of the liquid phase.

In Fig. 10 the effect of a weak transverse magnetic field with Hartman-number $M^2 = 20.0$ ($B = 0.11$ T) in combination with solidification is shown. The scale length of the applied magnetic field is chosen such that the field grows smoothly from zero up to its maximum in a distance of $20a^*$. The action of the magnetic field is to compress the steady wave pattern and to decrease the braking length. The final state of uniform velocity and thickness is reached after approximately $400a^*$ (1.6 m).

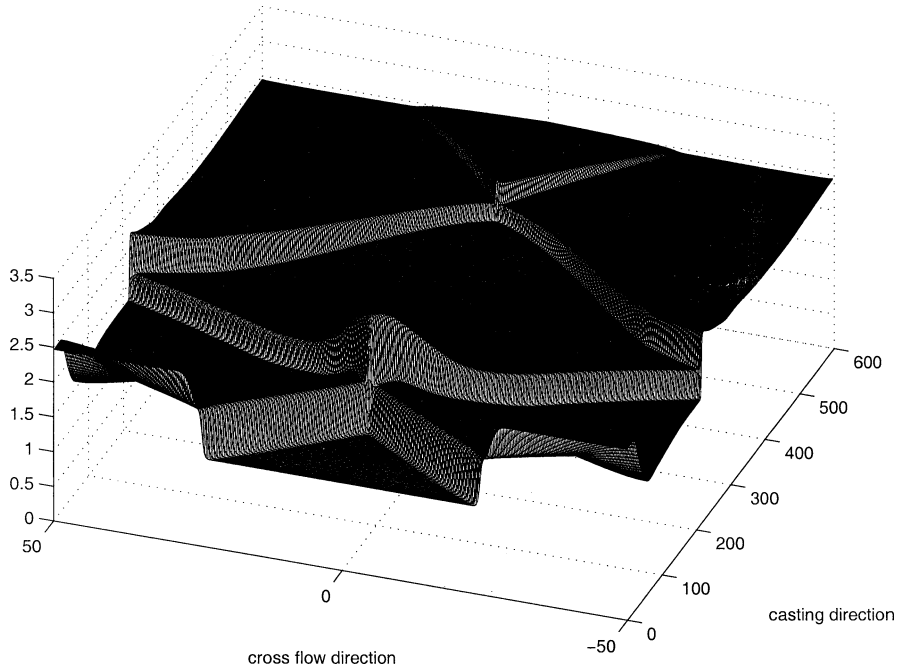

Fig. 9. The free-surface level with no magnetic field $M^2 = 0$, $R = 4500$, $F^2 = 32$ and solidification.

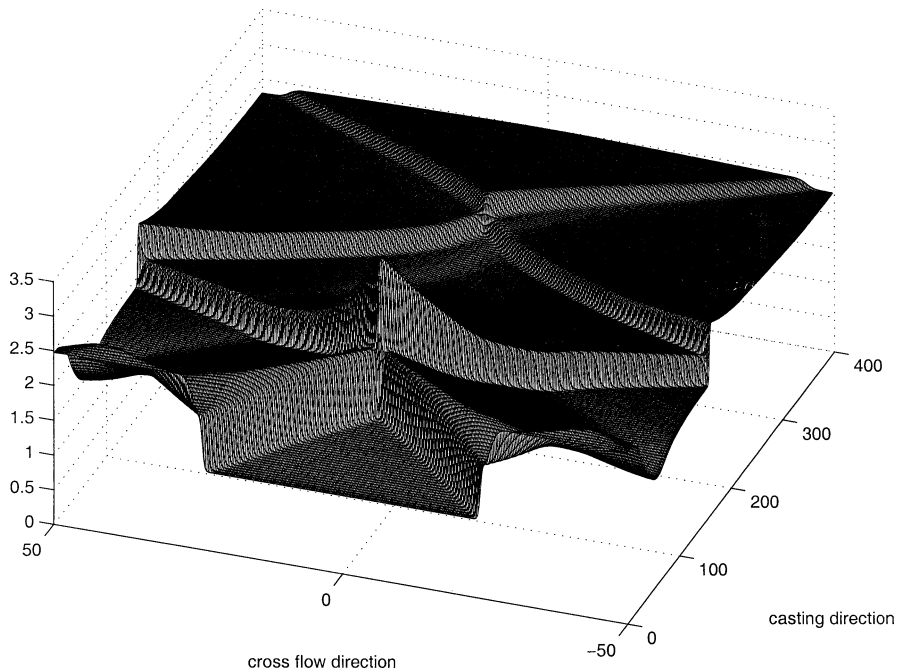

Fig. 10. Free-surface level distribution $h(x, y)$ with a solidifying phase but with magnetic field. Parameters $R = 4500$, $F^2 = 32$, $\beta = 0.4$, $M^2 = 20$.

Increasing the magnetic further to $M^2 = 30$ ($B = 0.13$ T) (Fig. 11) a smooth plane surface is obtained after a distance of $320a^*$ (1.3 m).

In Fig. 12 the magnetic field is increased to $M^2 = 40$ ($B = 0.155$ T). The braking distance is now of the order of the width of the copper belt, i.e., $130a^*$ (0.5 m). This should be considered as the minimum braking distance since the non-uniform region

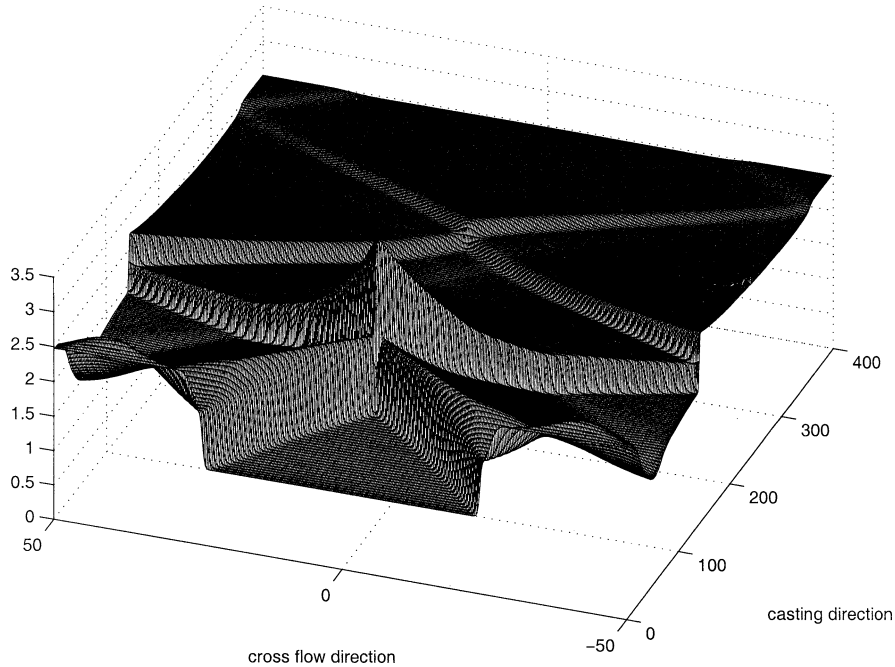

Fig. 11. Free-surface level distribution $h(x, y)$ magnetic field $M^2 = 30$ and solidification. Parameters $R = 4500,\ F^2 = 32,\ \beta = 0.4,\ M^2 = 30$.

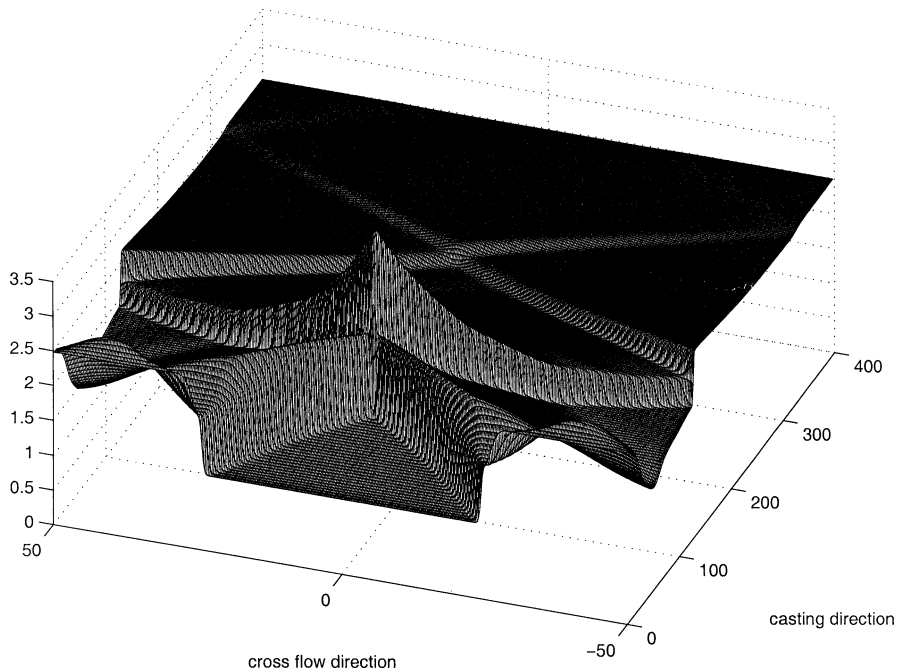

Fig. 12. Free-surface level distribution $h(x, y)$ magnetic field $M^2 = 40$ and solidification. Parameters $R = 4500,\ F^2 = 32,\ \beta = 0.4,\ M^2 = 40$.

of the electromagnetic force is of the order of the belt width. It is therefore no point in increasing the magnetic field further beyond say $M^2 = 40$.

In the second case we consider oblique feeding in which 80% of the plane jet is fed directly into the casting direction. This corresponds to an impinging jet striking the surface at an angle of 53°with respect to the horizontal. The volume flux is the same as in the previous case. In Figs. 13 and 14 the case with solidification and different magnetic fields ($M^2 = 20, 40$) are

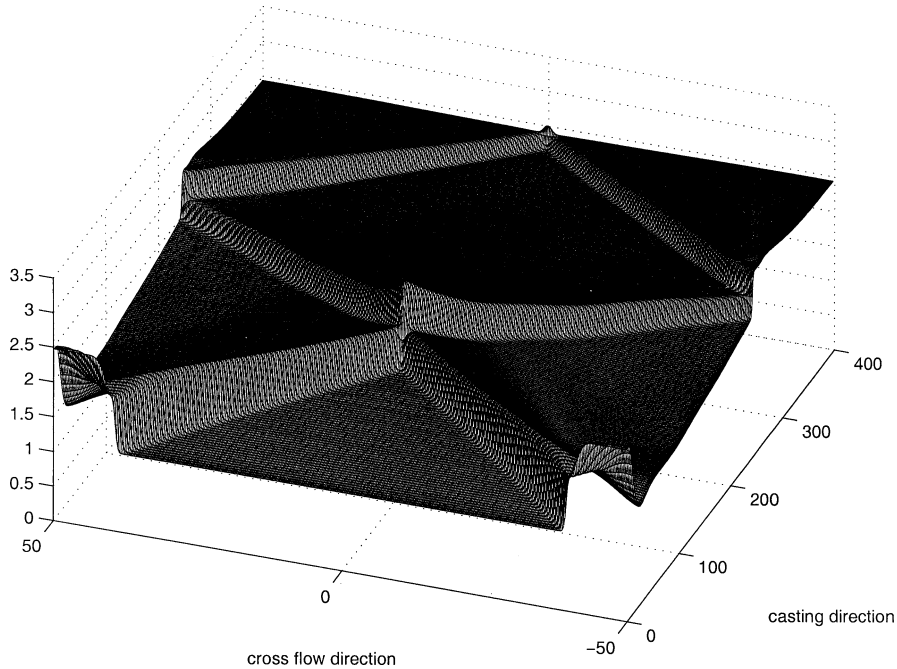

Fig. 13. Free-surface level $h(x, y)$ for the case of magnetic field $M^2 = 20$ and solidification. Oblique feeding. Parameters $R = 4500$, $F^2 = 32$, $\beta = 0.4$, $M^2 = 20$.

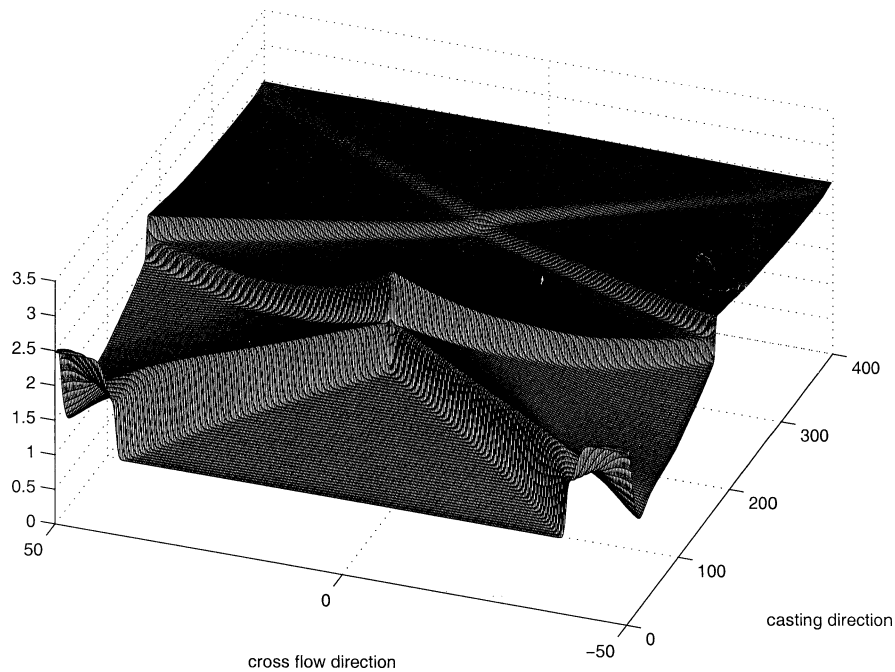

Fig. 14. Free-surface level $h(x, y)$ for the case of magnetic field $M^2 = 40$ and solidification. Oblique feeding. Parameters $R = 4500$, $F^2 = 32$, $\beta = 0.4$, $M^2 = 40$.

shown. Although the difference between the two different feeding techniques, feeding the liquid vertically or obliquely onto the belt is large for the case with no magnetic field, this difference is with the application of a magnetic field smoothed out after a length of the order of the belt width.

5. Conclusions

The three-dimensional liquid metal flow typically occurring in the industrial process of horizontal belt strip casting is considered. The investigation includes effects from a transverse magnetic field as well as a growing solidifying phase beneath the liquid phase. In the entrance of the liquid metal into the transverse magnetic field, electric fields and currents are induced. This results in an entrance region with a largely varying electromagnetic force. The size of this region is of the order of the width of the belt. After the entrance region there is a uniform braking force from the electromagnetic field. The final state corresponds to a uniform velocity equal to the belt and uniform thickness, which is favorable for the stability and the solidification.

Cases where the flow is supercritical are analyzed numerically. Supercritical flow is necessary in a commercial application of the process. The initial flow after the feeding jet is assumed to consist of a central part with large velocity and shallow thickness. A somewhat thicker liquid and a velocity equal to the belt characterize the flanks. The numerical results show that without magnetic field and no solidification, the non-uniform initial conditions, produced from the feeding, are propagating in the form of steady hydraulic jumps. These jumps are reflected at the sidewalls and are only weakly damped downstream by viscous dissipation. With the inclusion of a transverse magnetic field of the order of 0.16 T and the presence of a growing solidified phase, the braking distance becomes considerably shorter and the damping of steady waves substantial.

Two cases of feeding the liquid metal on the belt are considered. In the first case the jet is fed vertically onto the belt, giving rise to a strongly non-uniform distribution of liquid on the belt. Approximately half of the jet is then spread directly into the casting direction, whereas the other half enter into the casting direction at the flanks, after first being spread in a direction opposite to the casting direction. For this case without a magnetic field, the steady waves produced from the propagation of the initial distribution have large amplitude. In the second case considered the liquid is fed obliquely onto the belt with an angle 53° with respect to the horizontal. The main part of the liquid (80%) is then spread directly into the casting direction. In this case the perturbation of the main flow from the back flow is less, leading to weaker amplitude of the steady waves propagating downstream. Applying a magnetic field of strength of 0.15 T, these differences in the initial distribution are largely erased after a distance of the order of the belt width. There is however no point in increasing the magnetic field above this value, because there is always a region at the entrance into the magnetic field in which the electromagnetic force is non-uniform. With the application of the transverse magnetic field, we therefore have a general method to damp out disturbances occurring in the feeding region, and there is therefore a large possibility that an even plane surface can be accomplished before the point of complete solidification.

Acknowledgements

The authors are grateful for discussions with Bernhard Müller concerning the use of Riemann solvers for system of hyperbolic equations. The research is sponsored by Norrbottens forskningsråd and the Swedish Research Council for Engineering Sciences (TFR).

Appendix. Numerical method

In the numerical method one starts with a set of discrete mesh points $(x, y) = (x_n, y_j) = (n\Delta x, j\Delta y)$. The approximate solution at (x_n, y_j) is denoted $\mathbf{F}_j^n$ and is considered constant in each cell $[y_j - \Delta y/2, y_j + \Delta y/2]$. The nonlinear system (2.17) is then linearized and at each cell interface $y_{j-1/2} = \frac{1}{2}(y_{j-1} + y_j)$ a local Riemann problem is solved. Eq. (2.17) then becomes

$$\frac{\partial \mathbf{F}}{\partial x} + \tilde{\mathbf{A}}_{j-1/2}(\mathbf{F}_{j-1}, \mathbf{F}_j) \cdot \frac{\partial \mathbf{F}}{\partial y} = \mathbf{H}. \tag{A.1}$$

The Jacobian $\tilde{\mathbf{A}} = \tilde{\mathbf{A}}_{j-1/2}(\mathbf{F}_{j-1}, \mathbf{F}_j)$ is approximated according to Roe to fulfill the following three conditions

$$\begin{aligned} &\text{(i)} \quad \tilde{\mathbf{A}} \cdot (\mathbf{F}_j - \mathbf{F}_{j-1}) = \mathbf{G}(\mathbf{F}_j) - \mathbf{G}(\mathbf{F}_{j-1}) \quad \Leftrightarrow \quad \tilde{\mathbf{A}} \cdot \Delta\mathbf{F} = \Delta\mathbf{G}, \\ &\text{(ii)} \quad \tilde{\mathbf{A}}_{j-1/2}(\mathbf{F}_{j-1}, \mathbf{F}_j) \text{ is diagonalizable with real eigenvalues,} \\ &\text{(iii)} \quad \tilde{\mathbf{A}}_{j-1/2}(\mathbf{F}_{j-1}, \mathbf{F}_j) \to \frac{\partial \mathbf{G}}{\partial \mathbf{F}}\big(\overline{\mathbf{F}}\big) \quad \text{as } \mathbf{F}_j, \mathbf{F}_{j-1} \to \overline{\mathbf{F}}. \end{aligned} \tag{A.2}$$

The first condition takes care of the case when there is a discontinuity (shock or hydraulic jump) separating the two values at the left $\mathbf{F}_\mathrm{L}$ and to the right $\mathbf{F}_\mathrm{R}$. Across the discontinuity a Rankine–Hugoniot condition should be satisfied so that

$$\Delta\mathbf{G} = \mathbf{G}(\mathbf{F}_\mathrm{R}) - \mathbf{G}(\mathbf{F}_\mathrm{L}) = s(\mathbf{F}_\mathrm{R} - \mathbf{F}_\mathrm{L}) = s\Delta\mathbf{F}, \tag{A.3}$$

where s is the "speed" (or tangent of the local characteristic) of the discontinuity. Together with condition (i) this shows that s is an eigenvalue of the approximate Jacobian

$$\tilde{\mathbf{A}} = \tilde{\mathbf{A}}_{j-1/2}(\mathbf{F}_{j-1}, \mathbf{F}_j) = \tilde{\mathbf{A}}_{j-1/2}(\mathbf{F}_\mathrm{L}, \mathbf{F}_\mathrm{R}). \tag{A.4}$$

Condition (ii) is the condition for a hyperbolic problem and condition (iii) ensures that it is a good approximation to the derivative when $\mathbf{F}_\mathrm{R}$ and $\mathbf{F}_\mathrm{L}$ are close.

A construction of such an approximate Jacobian for Eulers equations was first given by Roe [16]. A construction of an approximate Jacobian for the system (2.5) will be given below.

The numerical scheme to solve (2.5) is a finite difference discretisation with upwind differencing for waves propagating to the left, corresponding to positive eigenvalues of the Jacobian and downwind differencing for waves propagating to the right, corresponding to negative eigenvalues (see Glaister [17]).

The jump condition across a discontinuity is given by

$$\Delta\mathbf{G} = \mathbf{G}(\mathbf{F}_\mathrm{R}) - \mathbf{G}(\mathbf{F}_\mathrm{L}) = \lambda(\mathbf{F}_\mathrm{R} - \mathbf{F}_\mathrm{L}) = \lambda\Delta\mathbf{F}, \tag{A.5}$$

where λ is an eigenvalue of the Jacobian and also the local value of the tangent $\mathrm{d}y/\mathrm{d}x$ of the characteristic. Since the Roe-matrix $\mathbf{A}$ is chosen such that

$$\Delta\mathbf{G} = \mathbf{A}\cdot\Delta\mathbf{F} = \lambda\Delta\mathbf{F} \tag{A.6}$$

we also note that $\Delta\mathbf{F}$ is an eigenvector of the matrix $\mathbf{A}$.

It is convenient to write the jump in $\mathbf{F}$ and $\mathbf{G}$ in terms of the jump of the primitive

$$\text{variables } \mathbf{q} = [\,\tilde{h} \quad U \quad V\,]^\mathrm{T}. \tag{A.7}$$

So that

$$\Delta\mathbf{F} = \widetilde{\mathbf{B}}\cdot\Delta\mathbf{q} \quad \text{and} \quad \Delta\mathbf{G} = \widetilde{\mathbf{C}}\cdot\Delta\mathbf{q}. \tag{A.8}$$

Matrices $\widetilde{\mathbf{B}}$ and $\widetilde{\mathbf{C}}$ fulfilling these conditions are given by

$$\widetilde{\mathbf{B}} = \begin{bmatrix} a\langle U\rangle + b\beta & a\langle\tilde{h}\rangle & 0 \\ c\langle U^2\rangle + e\beta^2 + d\beta\langle U\rangle + \frac{\langle\tilde{h}\rangle}{F^2} & 2c\langle\tilde{h}\rangle\langle U\rangle + d\beta\langle\tilde{h}\rangle & 0 \\ c\langle UV\rangle + \frac{d}{2}\beta\langle V\rangle & c\langle\tilde{h}\rangle\langle V\rangle & c\langle h\rangle\langle U\rangle + \frac{d}{2}\beta\langle\tilde{h}\rangle \end{bmatrix}, \tag{A.9}$$

$$\widetilde{\mathbf{C}} = \begin{bmatrix} a\langle V\rangle & 0 & a\langle\tilde{h}\rangle \\ c\langle UV\rangle + \frac{d}{2}\beta\langle V\rangle & c\langle\tilde{h}\rangle\langle V\rangle & c\langle h\rangle\langle U\rangle + \frac{d}{2}\beta\langle\tilde{h}\rangle \\ c\langle V^2\rangle + \frac{\langle\tilde{h}\rangle}{F^2} & 0 & 2c\langle\tilde{h}\rangle\langle V\rangle \end{bmatrix}, \tag{A.10}$$

where the following notation has been used

$$\langle q\rangle = \frac{1}{2}(q_\mathrm{R} + q_\mathrm{L}), \qquad \langle q^2\rangle = 2\langle q\rangle^2 - \hat{q}^2, \qquad \hat{q} = \sqrt{q_\mathrm{R}q_\mathrm{L}}. \tag{A.11}$$

Using (A6) and (A8) we find the Roe-matrix $\tilde{\mathbf{A}} = \widetilde{\mathbf{C}}\cdot\widetilde{\mathbf{B}}^{-1}$.

The eigenvalues of the matrix $\tilde{\mathbf{A}}$ are given by the equation

$$\left(\lambda - \frac{\langle V\rangle}{\langle U\rangle + (d/(2c))\beta}\right)\left(A_1\lambda^2 + 2A_2\lambda + A_3\right) = 0,$$

where

$$\begin{aligned} A_1 &= \beta^2(ae - bd) - 2bc\beta\langle U\rangle - ac\hat{U}^2 + \frac{a\langle\tilde{h}\rangle}{F^2}, \\ A_2 &= ac\left(2\langle U\rangle\langle V\rangle - \langle UV\rangle\right) + bc\beta\langle V\rangle, \\ A_3 &= \frac{a\langle\tilde{h}\rangle}{F^2} - ac\hat{V}^2. \end{aligned} \tag{A.12}$$

References

[1] R. Nyström, E. Burström, W. Reichelt, U. Urlau, DSC: A high-productivity concept for strip production of steel, in: Metec 94, 2nd European Conference on Continuous Casting, Düsseldorf, Steel Res. 64 (1994) 300–306.
[2] R.I.L. Guthrie, M. Hasan, C. Jefferies, R.P. Tavares, H. Murakami, Turbulent flow, heat transfer and solidification in thin strip casting machines, in: J.J. Jonas, N. Sano (Eds.), Sec. Canada–Japan Symp. on Modern Steelmaking and Casting Techniques, The Metallurg. Soc. of the Canad. Inst. of Mining, Metallurgy and Petroleum, August 20–25, 1994, pp. 201–219.
[3] N.A. Holmberg, Metal feeding in horizontal belt strip casters, Lic. thesis, Univ. of Luleå, 1996.
[4] N.A. Holmberg, Distribution of metal onto the belt of a horizontal strip caster, Steel Res. 69 (1) (1998) 22–27.
[5] H.B. Löfgren, H.O. Åkerstedt, Electromagnetic braking of a liquid metal flow with a free surface, Fluid Dynamics Res. 23 (1998) 1–25.
[6] H.B. Löfgren, H.O. Åkerstedt, Damping mechanisms of perturbations in electromagnetically braked horizontal film flows, Fluid Dynamics Res. 26 (2000) 53–68.
[7] H.B. Löfgren, H.O. Åkerstedt, The laminar stagnation-pointflow against a solidifying moving shell, Acta Mech. 142 (2000) 33–46.
[8] H.B. Löfgren, H.O. Åkerstedt, Initial solidification in liquid metal film flow over a moving boundary, Int. J. Heat Mass Transfer 44 (2001) 837–842.
[9] H.B. Löfgren, Ideal solidification of a liquid metal boundary layer flow over a conveying substrate, J. Fluid Mech. 446 (2001) 121–131.
[10] P.H. Steen, C. Karcher, Fluid mechanics of spin casting of metals, Ann. Rev. Fluid. Mech. 29 (1997) 373–397.
[11] A. Garcia, T.W. Clyne, M. Prates, Mathematical model for the unidirectional solidification of metals: II Massive molds, Metall. Trans. B 10 (1979) 85.
[12] R. Moreau, Magnetohydrodynamics, Kluwer Academic, 1990.
[13] J.A. Shercliff, A Textbook of Magnetohydrodynamics, Pergamon Press, 1965.
[14] E.F. Toro, Shock-Capturing Methods for Free-Surface Flows, Wiley, 2001.
[15] R.J. Leveque, Numerical Methods for Conservation Laws, Birkhäuser, 1994.
[16] P.L. Roe, Approximate Riemann solvers, parameter vectors, and difference schemes, J. Comput. Phys. 43 (1981) 357–372.
[17] P. Glaister, Approximate Riemann solutions of the shallow water equations, J. Hydraulic Res. 23 (3) (1988) 293–306.
[18] P.L. Roe, Upwind difference schemes for hyperbolic conservation laws with source terms, in: Carasso, Raviart, Serre (Eds.), Proc. First International Conference on Hyperbolic Problems, Springer, 1986, pp. 41–51.
[19] P. Glaister, Prediction of steady, supercritical, free-surface flow, Int. J. Engrg. Sci. 33 (1995) 845–854.
[20] R.J. Leveque, Balancing source terms and flux gradients in a high resolution Godunov methods: the quasi-steady wave-propagation algorithm, J. Comput. Phys. 146 (1998) 346–365.
[21] J.Y. Yang, S.H. Chang, W.H. Hui, A new Lagrangian method for steady supercritical shallow water flow computation, Comput. Methods Appl. Mech. Engrg. 104 (1993) 333–355.